Eur. J. Mineral., 38, 545–556, 2026
https://doi.org/10.5194/ejm-38-545-2026

European Journal of Mineralogy
Open Access

The impact of exsolution textures in Fe–Ti oxide minerals on crushing strategies and vanadium and titanium pre-concentration

Thomas Daniel van Gerve[1], **Philippe Muchez**[1], **Ted Nuorivaara**[2], **and Olivier Namur**[1]

[1]KU Leuven, Department of Earth and Environmental Science, Celestijnenlaan 200E, 3001 Leuven, Belgium
[2]Geological Survey of Finland, P.O. Box 96, 02151 Espoo, Finland

Correspondence: Olivier Namur (olivier.namur@kuleuven.be)

Received: 6 January 2026 – Revised: 19 June 2026 – Accepted: 7 July 2026 – Published: 21 August 2026

Abstract. Vanadiferous titanomagnetite (VTM) ores in mafic layered intrusions host the world's largest vanadium resources, with the Bushveld Complex representing the principal global deposit. This study examines the mineral textures and element redistributions in magnetite–ilmenite assemblages from Bushveld Upper Zone magnetites. Two main magnetite exsolution microstructures are identified: cloth textures dominated by ulvöspinel lamellae and sandwich or trellis textures characterized by ilmenite lamellae formed through ulvöspinel oxidation. In situ elemental analyses demonstrate that vanadium is concentrated in magnetite relative to ilmenite and that oxidation-driven exsolution enhances V enrichment in residual magnetite while concentrating Ti into ilmenite. The textural type strongly controls liberation potential: cloth textures exhibit pervasive fine intergrowths that hinder beneficiation, whereas sandwich and trellis textures show coarser separable lamellae. These microstructural variations have direct implications for magnetic, gravity, and flotation processing efficiency. The results highlight the necessity of textural characterization to optimize V–Ti ore beneficiation strategies.

1 Introduction

Vanadiferous titanomagnetite (VTM) deposits are accumulations of magnetite ± ilmenite and are the primary source of vanadium worldwide (Kelley et al., 2017). They are mainly found in mafic layered intrusions (MLIs), which comprise Mg- and Fe-rich cumulate rocks with prominent mineralogical layering (Charlier et al., 2015a; Namur et al., 2015; Latypov et al., 2024). Past and current exploited MLIs include the Bushveld Complex (South Africa; Cawthorn and Molyneux, 1986), the Emeishan large igneous province (China; Zhou et al., 2005), the Windimurra complex (Australia; Mathison and Ahmat, 1996), and the Lac Doré complex (Canada; Taner et al., 1998). Other large MLIs are currently being evaluated for future exploitation (e.g. Sept Iles, Canada; Namur et al., 2010, 2012). Bushveld is economically the most significant and hosts the largest VTM deposit worldwide, with one of the highest vanadium ore grades of up to 1.5 wt % V_2O_5 (Kelley et al., 2017), and, as a result, Bushveld holds ∼ 30 % of the world's total vanadium reserves (Taylor et al., 2009).

Depending on their Ti, Fe, and V contents, VTM ores are processed in various ways (Taylor et al., 2006), but they all involve milling and/or crushing and magnetic mineral separation steps aimed at improving mineral liberation and ore grade. Macroscopic and microscopic mineral textures influence liberation degrees and potentially affect the quality of resulting processed products. Structural properties such as grain size, intergrowths, microcracks, exsolution textures, inclusions, oxidation states, and surface defects influence the response of these minerals to comminution and subsequent separation stages (Månbro et al., 2025). For example, changes in mineral compositions and inclusions within ilmenite or magnetite grains can change their effective density, impairing gravity separation efficiency (Abaka-Wood et al., 2019). Magnetic properties are also affected by oxidation states and mineralogical composition, which influence magnetic susceptibility and, consequently, the effectiveness of magnetic separation (Zhitao and Kuangdi, 2022). Finally, in froth flotation, the liberation of the target mineral, typically ilmenite in such ores, is essential for proper separation to occur (Wills and Finch, 2015).

The aims of this study are (1) to describe the variety of textures present in the Fe–Ti oxide minerals in the ore; (2) to determine the relationship between the textures and the chemical composition of the different minerals in these specific textures; and (3) to document, based on the current knowledge of ore processing, the impact of the mineral textures on the degree of liberation and concentration. In order to obtain these goals, the Bushveld Complex has been selected as an important case study since this is the most significant VTM deposit worldwide.

1.1 Bushveld geological setting and samples

The Bushveld Complex is located in South Africa and is the largest mafic layered intrusion in the world, covering 65 000 km^2 (Fig. 1). It was emplaced between 2.5 and 2.06 Ga within sedimentary host rocks (Zeh et al., 2015) and consists of several suites, but the V–Ti deposits are mainly found in the mafic Rustenburg Layered Suite (RLS, Fig. 1). The RLS comprises (from bottom to top) the Lower, Critical, Main, and Upper zones (Cawthorn, 2015). The Lower and Critical zones crystallized from primitive, Mg-rich magmas, and the Main Zone crystallized from a more tholeiitic, Fe-rich magma, while the Upper Zone is derived from residuals of these earlier liquids (Eales and Cawthorn, 1996). Magnetite is mainly found near the top of the RLS, and its first appearance is often used to define the boundary between the Main and Upper zones (Molyneux, 1974; Scoon and Mitchell, 2012; Yuan et al., 2017). The Main and Upper zones transition from gabbronorites to Fe–Ti-oxide gabbros and host up to 30 magnetite- and ilmenite ± apatite-rich layers. These magnetite layers are laterally continuous over large distances, potentially tens or hundreds of kilometres, and, as a result, V–Ti deposits are found in most areas where the Upper zone is exposed or occur near the surface. Due to lateral extent of the magnetite-rich layers, as well as the lateral homogeneity in terms of thickness, texture, and likely mineral compositions (e.g. Reynolds, 1985), single samples from such layers are representative of a large extent of the Bushveld Complex. We therefore use seven samples of magnetite-rich rocks (Table S1 in the Supplement) from a drillcore in the western limb of the complex to study Bushveld mineral textures (BK3; Fig. 1). The whole-rock composition and the compositions of silicate minerals have been described previously (Yuan et al., 2017).

1.2 Magnetite and ilmenite mineral textures

In the Bushveld Complex, magnetite and ilmenite are the dominant V and Ti ore minerals, respectively. Their compositions are dominated by Ti and Fe, but they also contain V, Al, Mg, and Mn. Ilmenite has the general formula $A_xB_{2-x}O_3$, where Fe^{2+}, Fe^{3+}, and Ti act as substitutes on the A (Fe^{2+}, Fe^{3+}), and B (Fe^{3+}, Ti^{4+}) crystallographic sites. This forms a solid-solution series (ilm_{SS}) between pure ilmenite (ilm: $FeTiO_3$; all Fe as Fe^{2+}) and hematite (hem: Fe_2O_3; all Fe as Fe^{3+}) endmembers (Fig. 2), where the relative contributions of each endmember are usually expressed as mol fractions X_i, with $\sum X = 1$. As a result, ilm_{SS} can have a continuous range of compositions, varying from Ti-rich (maximum 35.86 wt % Fe for stoichiometric $FeTiO_3$) to Fe-rich (maximum 69.94 wt % Fe for stoichiometric Fe_2O_3) with decreasing X_{ilm} and increasing X_{hem}. While near-endmember compositions (X_{hem} or $X_{ilm} > 0.80$) are stable down to low temperatures (< 500 °C), more equal mixtures ($0.30 < X_{hem}$, $X_{ilm} < 0.7$) are unstable below ∼ 900 °C (Buddington and Lindsley, 1964; Lindsley, 1991). As a result, cooling below this temperature leads to exsolution into near-endmember compositions becoming increasingly closer to the endmember compositions with decreasing temperature (Buddington and Lindsley, 1964; Carmichael, 1961).

Magnetite has the general formula $A_xB_{3-x}O_4$, which mainly forms a solid solution series (mtss) between Ti-rich ulvöspinel (usp: Fe_2TiO_4, with all Fe as Fe^{2+}) and Fe-rich magnetite (mt: Fe_3O_4, with one Fe^{2+} and two Fe^{3+} per formula unit) endmembers (Fig. 2). However, natural magnetite can incorporate other elements like Al and Mg, potentially forming more complex solid solutions with additional components, e.g. hercynite ($FeAl_2O_4$) or spinel ($MgAl_2O_4$; Turnock and Eugster, 1962; Charlier et al., 2015; Arguin et al., 2018). During progressive cooling, mt solid solutions become unstable at low temperatures and exsolve (Buddington and Lindsley, 1964). Exsolution temperatures depend on the components involved and vary from < 600 °C for magnetite–ulvöspinel solid solution (Buddington and Lindsley, 1964) to ∼ 860 °C for hercynite–magnetite solid solution (Turnock and Eugster, 1962). In addition to exsolution, ulvöspinel components in magnetite can oxidize and produce ilmenite + magnetite according to the following reaction (Buddington and Lindsley, 1964; Duchesne, 1970; Tan et al., 2016):

$$6Fe_2TiO_4\,(usp) + O_2 \rightarrow 6FeTiO_3\,(ilm) + 2Fe_3O_4\,(mt). \quad (1)$$

This oxidation therefore leads to the formation of near-endmember mt and ilm, i.e. mineral purification (Charlier et al., 2015b), and can be expressed as an intermediate between mt and ilm.

Ilmenite and magnetite exsolutions create intricate mineral textures made up of intergrowths of the near-endmembers of their respective solid-solution series. For magnetite, these textures may be complicated further by ulvöspinel oxidation. As a result, different mineral textures form depending on (1) the extent of exsolution and oxidation, (2) the bulk composition of the host minerals, and (3) the potential occurrence of subsequent processes like diffusive re-equilibration. Note that rates of exsolution and oxidation are also diffusion controlled and depend on the diffusion coefficients of all involved elements. If ilmenite formed through ion exchange,

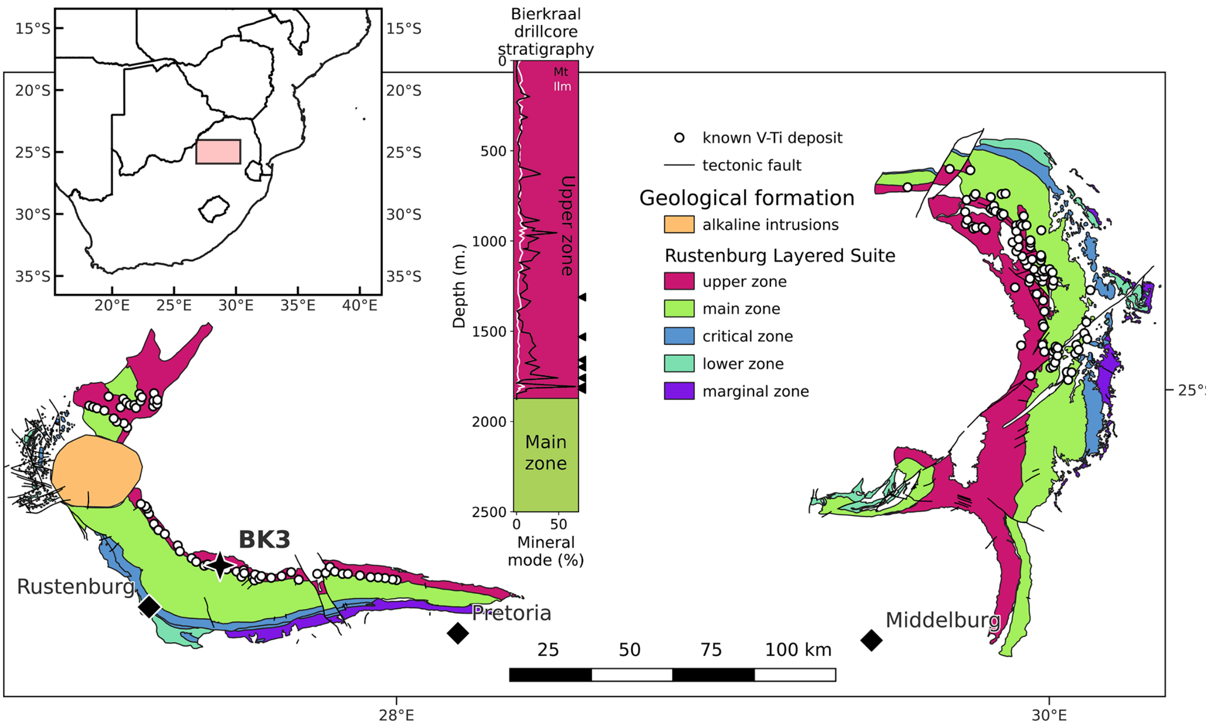

Figure 1. Geological map of the Bushveld Complex (BVC) in southern Africa (inset), showing the distribution of the Rustenburg Layered Suite (RLS) zones (marginal, lower, critical, main, and upper zones), alkaline intrusions, and tectonic faults. The map also locates known V–Ti deposits (open circles) associated with the RLS. The central panel displays the Bierkraal drillcore stratigraphy (depth in metres), illustrating the contact between the Upper and Main zones and showing the associated mineral mode percentages for Mt (Magnetite) and Ilm (Ilmenite).

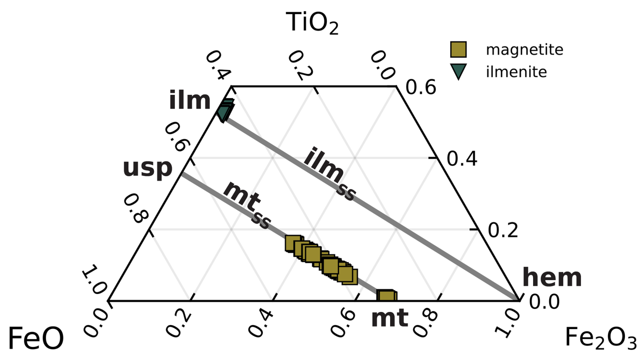

Figure 2. Ternary phase diagram illustrating the compositional fields and solid-solution series for oxide minerals. The vertices represent the pure end-member compositions FeO, Fe_2O_3, and TiO_2 (wt %). Grey lines represent the magnetite–ulvöspinel solid solution (mtss) and the ilmenite–hematite solid solution (ilmss). Symbols represent chemical analyses of the Bushveld Complex.

this would show as replacement textures at ulvöspinel grain boundaries (Charlier et al., 2015b, their Fig. 15). We do not observe such textures in Bushveld (see below) and have only found "classical" sandwich and trellis textures. We therefore do not think that ion exchange has contributed significantly to ilmenite formation.

2 Bushveld titanomagnetite and ilmenite textures

As described in Sect. 1.2, magnetite and ilmenite can display a range of complex macroscopic and microscopic textures (Arguin et al., 2018; Duchesne, 1970; Von Gruenewaldt et al., 1985). However, at Bushveld, ilmenite grains are homogeneous and show no visible textures due to their originally low X_{hem}. Contrastingly, Bushveld magnetites show a variety of textures, which can be divided into two main types: sandwich (or trellis) textures and cloth textures. The samples with cloth texture are all from stratigraphically lower positions (> 1500 m) than samples with trellis textures (< 1300 m). Magnetite grains with a sandwich texture are observed in samples also containing cloth-textured magnetite. For details on the textures of ilm_{SS} with high X_{hem}, we refer the readers to studies on other ilmenite-rich deposits (e.g. Charlier et al., 2009, 2015b).

2.1 Cloth textures

Magnetites with cloth textures in the Bushveld Complex show a 3D network of ulvöspinel lamellae along the (100), (010), and (001) crystallographic planes (Figs. 3 and 4; Price, 1980; Ramdohr, 1953; Tan et al., 2016). When crystals are cut parallel to one of the exsolution planes they intersect

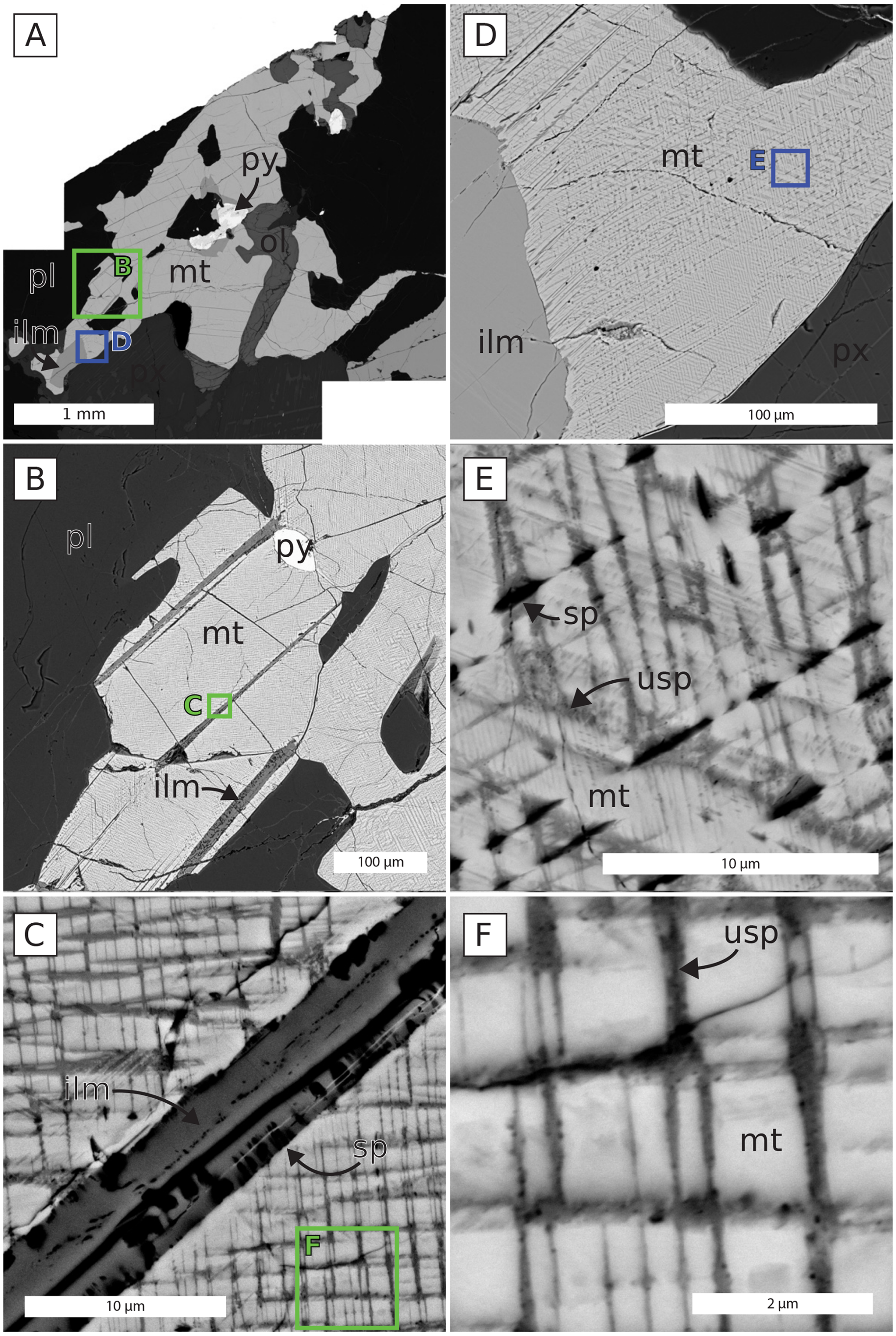

Figure 3. Back-scattered electron (BSE) images illustrating the textural relationships and solid-state exsolution features within oxide. **(A)** Low-magnification overview showing the primary assemblage of magnetite (mt), ilmenite (ilm), pyrite (py), olivine (ol), and plagioclase (pl). **(B)** Medium-magnification view showing the boundary relationships between magnetite and ilmenite lamellae. **(C)** High-magnification detail of magnetite hosting lamellae of ilmenite. **(D)** Medium-magnification view of a large magnetite grain displaying a pervasive network of exsolution lamellae, adjacent to ilmenite and pyroxene (px). **(E)** High-magnification detail of the magnetite from **(D)**, clearly showing a fine, crystallographically oriented, cloth-like texture of ulvöspinel (usp) lamellae exsolved within the magnetite host. **(F)** High-magnification image showing the detailed network of ulvöspinel (usp) lamellae within the magnetite host from area **(C)**.

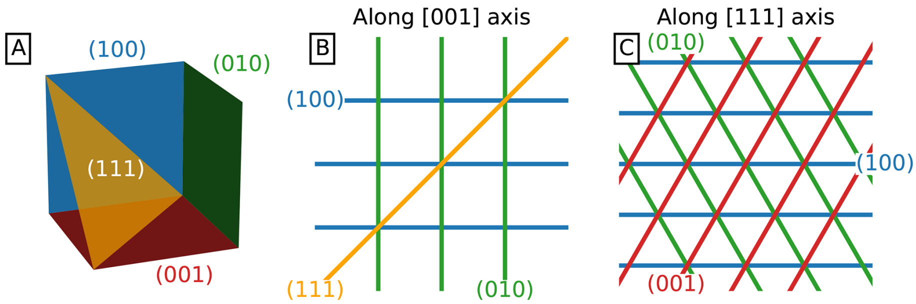

Figure 4. Orientations of crystallographic planes in magnetite **(A)**. Oxidized sandwich and trellis ilmenite form along the {111} set, and exsolved cloth ulvöspinel forms along the (100), (010), and (001) planes. **(B)** Typical occurrence of sandwich ilmenite along a single {111} plane (yellow), with interstitial cloth ulvöspinel along the (100) and (010) planes. Observed angles between the various planes depend on the cross-section angle. For the (100) and (010) planes they are 90° from cut parallel to the (001) plane **(B)** and 60–120° when cut parallel to the (111) plane **(C)**.

at 90° in cross-section (Figs. 3c, f and 4b), but when crystals are cut along the [111] crystallographic axis they show 60–120° intersections (Figs. 3d, e and 4c). These lamellae are a few micrometres to nanometres thick, and their spacing ranges from ca. 0.1 to 3 µm. Granular and needle-like Al-rich (hercynitic) spinel [$(Mg,Fe)Al_2O_4$] of up to 3 µm in length is sometimes associated with these lamellae (Fig. 3e; Spencer and Lindsley, 1981; Charlier et al., 2015b). This may indicate evolution along the magnetite–ulvöspinel–Al–spinel solid-solution series (e.g. Charlier et al., 2015b) and implies solvus temperatures higher than those of magnetite–ilmenite solid solution (see Sect. 1.2). However, the modal abundances of spinel in cloth-textured magnetite are very low ($\ll 1$ %), and its impact is therefore expected to be minor. At Bushveld, cloth textures are often observed in interstitial magnetite within grains with sandwich textures (see below) but never in grains with trellis textures (see below). Identical textures are found in VTM deposits worldwide and they form via exsolution as magnetite cools below the solvus (Arguin et al., 2018; Duchesne, 1972; Taner et al., 1998; Namur et al., 2010).

2.2 Sandwich and trellis textures

In the Bushveld Complex, magnetite sandwich or trellis texture are characterized by relatively thick, ~ 10–300 µm ilmenite lamellae inside magnetite grains, spaced tens to hundreds of micrometres apart. In the sandwich textures, lamellae are all roughly parallel (Fig. 5a and b), and the interstitial magnetite has pervasive cloth textures made up of thin ulvöspinel lamellae (see Sect. 2.2, Fig. 5a–c). Furthermore, granular ilmenite is sometimes found along grain boundaries of sandwich textured magnetite. Contrastingly, in the Bushveld trellis textures, ilmenite lamellae form along 2–3 different planes (Fig. 5a), with 60–120° angles between them. Here, the interstitial magnetite (mt) contains very thin (< 1 µm) and short (~ 10 µm), needle-like exsolutions of ilmenite and spinel (Fig. 5d). However, often a border array of spinel of ca. 10 µm is present around the trellis lamellae where these needles are mostly absent (Fig. 5b–d).

The ilmenite lamellae and needles form via oxidation of the ulvöspinel component in titanomagnetite according to Reaction (R1). In sandwich textures, they form along a single (111) plane (Fig. 4a and b), while they form along multiple sets of the {111} planes in trellis textures (Fig. 4a; Buddington and Lindsley, 1964; Haggerty, 1991; Mücke, 2003; Tan et al., 2016). Notably, the presence of ulvöspinel in the cloth texture of interstitial magnetite in sandwich textures indicates (1) that these magnetites were not completely oxidized and (2) that the sandwich ilmenite lamellae formed before the cloth texture.

The ilmenite-free zone around ilmenite trellis lamellae indicates that diffusion of Ti through titanomagnetite has taken place after oxidation. Through this process, the needle-like ilmenite is effectively transported towards the trellis lamellae, leaving behind an ilmenite-free border zone (Duchesne, 1970; Von Gruenewaldt et al., 1985). However, diffusion rates in the trellis textures were not high enough to have all ilmenite and spinel components migrate to the ilmenite lamellae, and, in more internal parts, the needles are therefore still present. Similarly, the observed granular ilmenites likely formed through diffusion near grain borders, expelling ilmenite from the magnetite grains (Duchesne, 1970; Namur et al., 2010).

3 Vanadium and titanium deportment

In Bushveld, both magnetite and ilmenite crystallized from a silicate melt. At magmatic temperature, vanadium and titanium partitioning varies between ilmenite and magnetite and their respective components (Shepherd et al., 2022). Vanadium is 3–4 times more compatible in $magnetite_{SS}$ than $ilmenite_{SS}$, and, under more reducing conditions (i.e. lower oxygen partial pressure), compatibility is enhanced for both minerals. Additionally, vanadium is about 2 times more compatible in endmember magnetite (mt) than ulvöspinel (Shep-

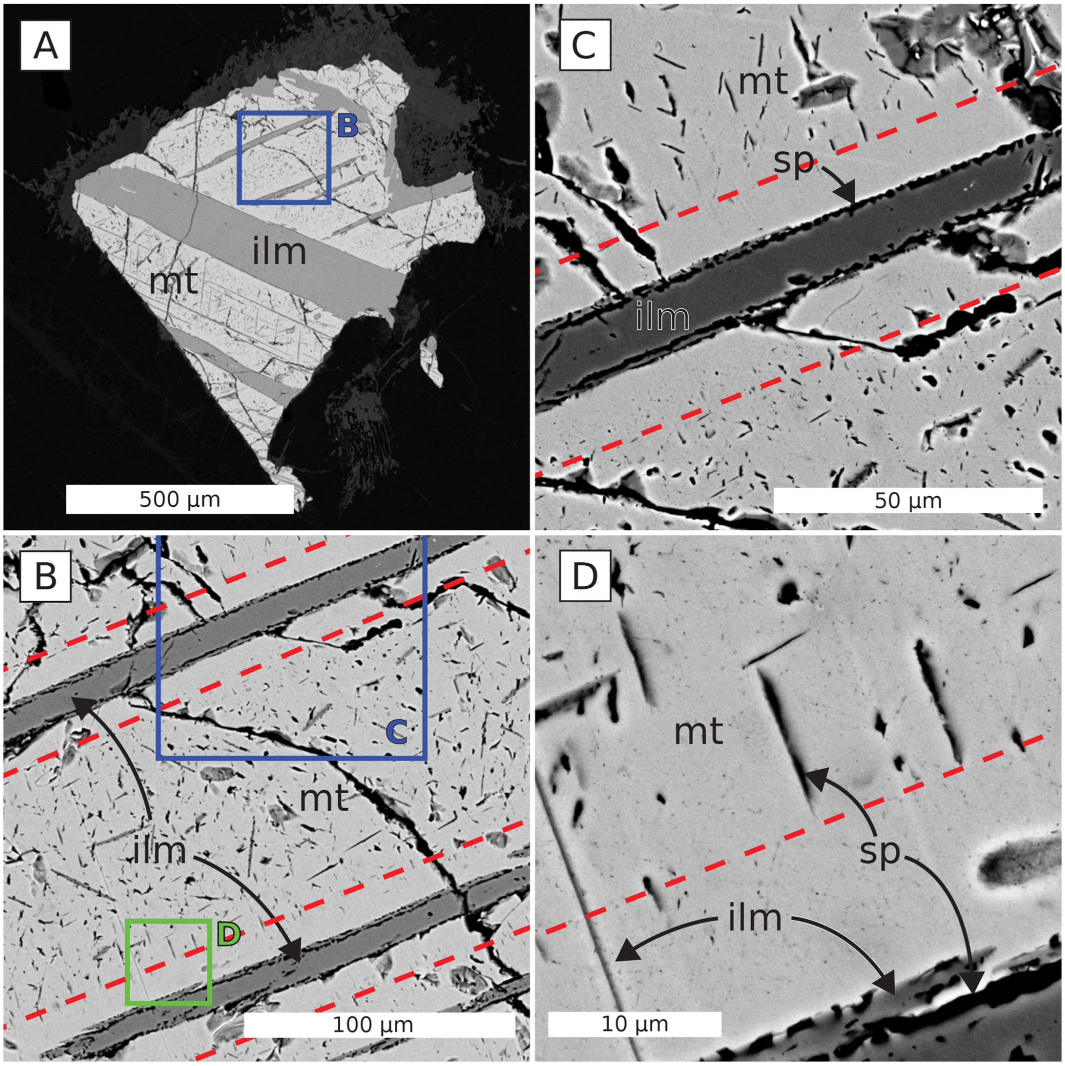

Figure 5. Back-scattered electron (BSE) images illustrating textural relationships in oxide minerals. **(A)** Low-magnification overview showing large intergrown crystals of ilmenite (ilm) and magnetite (mt). **(B)** Medium-magnification view detailing the interface between magnetite and ilmenite. The magnetite exhibits a clear, crystallographically controlled pattern of exsolution lamellae of ilmenite. **(C)** Higher-magnification view of the magnetite showing the pervasive fine granules of spinel exsolved at the magnetite-ilmenite interface. **(D)** High-magnification detail focusing on the spinel lamellae within the magnetite, demonstrating the fine-scale exsolution features and the absence of small spinel exsolutions in the vicinity of a large ilmenite lamella.

herd et al., 2022). As a result, vanadium preferentially distributes into magnetite (mt) during magnetite$_{SS}$ exsolution, while the exsolved ulvöspinel is comparatively V-poor. Additionally, ulvöspinel oxidation further enriches residual magnetite in V and produces V-poor ilmenite lamellae (Reaction R1). Ilmenite exsolution during full oxidation of magnetites therefore produces residual magnetite with the highest possible vanadium content (Fig. 6). Titanium compatibility also varies between the various minerals and components. Of all Bushveld ore minerals, the endmember ilmenite is the most Ti-rich and has the highest compatibility. During both ilmenite$_{SS}$ exsolution (forming hematite lamellae) and ulvöspinel oxidation, titanium is concentrated into ilmenite (ilm). Here, we investigate the extent of V and Ti (re)distribution resulting from mineral texture formation with in situ chemical analyses energy-dispersive X-ray (EDX) spectroscopy on prepared thin sections. The sections were polished with 1 µm polycrystalline diamond paste and were subsequently carbon coated with a thickness of 20 nm.

EDX analyses were performed on a Tescan MIRA 4 field emission gun scanning electron microscope (FEG-SEM) at KU Leuven. It is equipped with an Oxford Xplore 30 EDX detector and a 15 kV accelerating voltage, and a 6 nA beam current was used for the analyses. Measurements were quantified with the factory extended calibration dataset included in the Oxford Aztec software. Iron was measured as total FeO

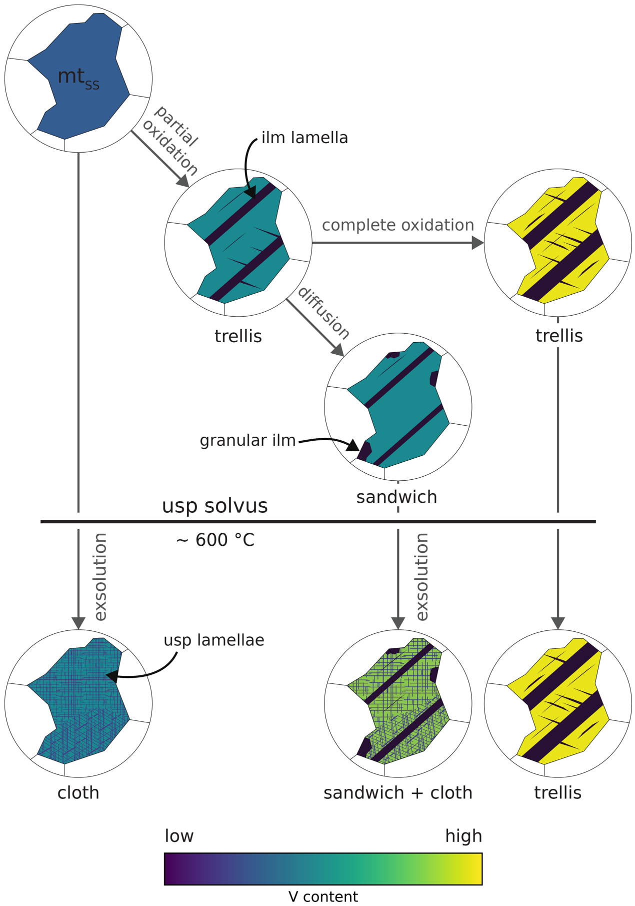

Figure 6. Changes in magnetite V content related to texture formation. At temperatures above the ulvöspinel solvus, oxidation of ulvöspinel components in mt_{SS} produces trellis ilmenite lamellae (Reaction R1). Ilmenite is V-poor, and V concentrations in residual magnetite increase with oxidation extents. Subsequent diffusive re-equilibration transports ilmenite towards grain boundaries and the main ilmenite lamellae, converting trellis into sandwich textures. Below 600 °C, remaining ulvöspinel components exsolve into end-member ulvöspinel and magnetite as cloth textures. While V is more compatible in magnetite than ulvöspinel, the difference is smaller than between magnetite and ilmenite. The V enrichment of exsolved magnetite is therefore less pronounced than that of oxidized magnetite. Consequently, full oxidation of mt_{SS} produces residual magnetite with the highest possible vanadium content.

and later converted into $Fe^{2+}O$ and $Fe^{3+}_2O_3$ according to the procedure by Andersen et al. (1993). Repeat measurements of secondary magnetite and ilmenite standards (Fig. S1, NMNH114887 and NMNH96189; Jarosewich, 2002) were used to estimate analytical precision and accuracy. Their results indicate that magnetite was measured with precisions and accuracies of < 1 % and < 4 % for major elements (but > 1 wt %). For ilmenite, major-element precision was < 3 %, except for Fe_2O_3, where it was ~ 9 %. Ilmenite major-element accuracies were < 4 %, except for Fe_2O_3 where it was 12.5 %. For minor elements (0.1 wt %–0.3 wt %), the accuracies and precision for ilmenite measurements were ~ 2 % and 6 %, while, for those in magnetite, they were both ≤ 50 %. V concentrations in magnetite from the Bushveld are > 0.3 wt %, and, as such, much lower accuracy is expected. In EDX spectra, V-$k\alpha$ and V-$k\beta$ peaks overlap, which potentially affects their measurements. In magnetite and ilmenite, where both elements are present, this may lead to overestimation of their V contents. If this is the case, positive correlations between Ti and V concentrations are expected. However, no positive correlations between TiO_2 and V_2O_5 concentrations were observed (Fig. S2), and V-$k\alpha$ and V-$k\beta$ peak overlap therefore had no or a negligible effect on measurement quality. Only analyses with totals of 97–103 wt % after $Fe^{2+}O$–$Fe^{3+}_2O_3$ conversion were included for magnetite, while for ilmenite a 97 wt %–104 wt % range was used. Relatively wide ranges of totals were included in order to account for the added uncertainty from $Fe^{2+}O$-$Fe^{3+}_2O_3$ calculations.

Cloth-textured lamellar exsolutions in magnetite are, at most, a few micrometres wide. This is below the typical spatial resolution of EDX spot analyses, and these exsolution therefore cannot be measured individually. Instead, their measurements are mixtures with the surrounding magnetite. Identifying whether the lamellae are ulvöspinel of ilmenite is therefore not straightforward. We used the Fe speciation and endmember component calculations from Andersen et al. (1993) to verify the dominant phase of the lamellae.

3.1 Sandwich and trellis textures

Analyses of the ilmenite and magnetite parts of trellis and sandwich textures show that they have near-endmember mt and ilm compositions (Fig. 7). This indicates that all ulvöspinel has been converted according to Reaction (R1) and that the magnetite has been fully oxidized into mt and ilm near-endmembers. Here, ilmenite exsolutions have V_2O_5 contents of 0.27 wt %–0.41 wt %, while, in the magnetite host, they are considerably higher at 0.72 wt %–1.14 wt % (Fig. 7). Before the formation of the trellis texture, these components were in solid solution, and the oxidation of the precursor magnetite therefore enriched the remaining magnetite in vanadium (Fig. 6). The downside of this process is that the formation of ilmenite trellis also reduces the degree of magnetite liberation. Since the grains with a trellis texture are fully oxidized, the amount of ilmenite lamellae reflects the composition of the precursor magnetite, where more lamellae indicate lower magnetite components formed at magmatic temperature. This means that trellis grains with fewer lamellae have higher overall V_2O_5 contents in addition to having more liberated magnetite.

V_2O_5 concentrations in trellis-textured magnetite are overall lower than those in cloth-textured host magnetite. As indicated above, the stratigraphic positions of trellis samples are higher than those with cloth textures. The samples with trellis textures therefore crystallized later, likely from magmas with overall lower vanadium contents (e.g. Yuan et al,

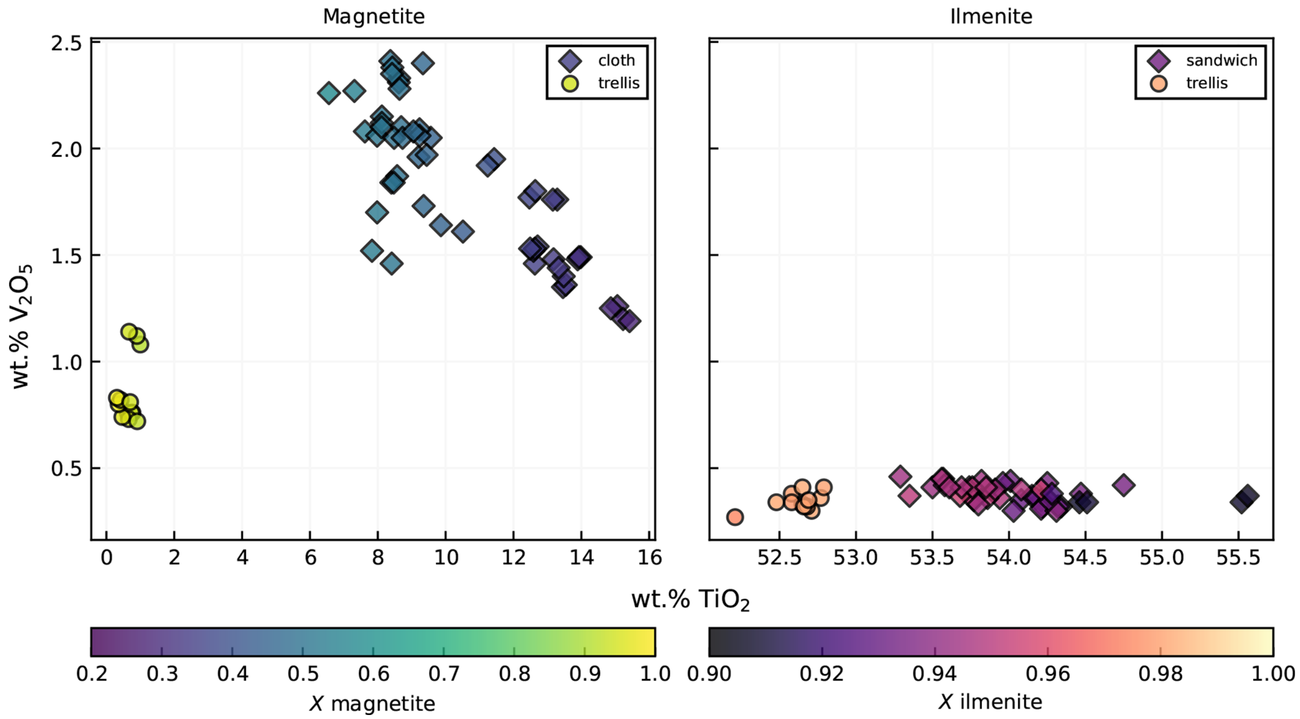

Figure 7. Compositional diagrams showing the V_2O_5 and TiO_2 content in magnetite and ilmenite from Bushveld. Symbols are colour-coded as a function of the magnetite fraction (X) in mt_{SS} and the ilmenite fraction in the ilm_{SS}.

2017; Namur and Humphreys, 2018). The lower vanadium concentrations in the trellis-textured magnetites are therefore a consequence of the overall lower V ore grade of these samples and not of element redistributions related to texture formation. Indeed, for magmatic mtss with the same bulk V_2O_5, the process of trellis formation is expected to enrich the mt host more than the process of cloth formation (Fig. 6). In trellis grains, TiO_2 concentrations in ilmenite lamellae are 52.2 wt %–52.8 wt % (i.e. near stoichiometric ilm), much higher than in any of the analysed magnetites (< 16 wt %). This shows that titanium effectively gets extracted from the mtss into ilm lamellae. In samples with sandwich lamellae, ilmenite exsolutions have comparatively low V_2O_5 contents of 0.3 wt %–0.46 wt % but high TiO_2 concentrations of 53.3 wt %–55.6 wt %.

3.2 Cloth textures

Chemical compositions of cloth lamellae and host magnetite can only be measured as mixtures of both as analytical spot sizes of currently available techniques for in situ chemical analyses are greater than the lamellae thickness and spacing. Measured compositions therefore depend not only on the $magnetite_{SS}$ compositions but also on the density of the exsolution network. Indeed, results from Bushveld show mixtures of endmember magnetite and ulvöspinel (i.e. compositions along the magnetite–ulvöspinel solid solution; Fig. 7). This is because there is no oxidation of ulvöspinel to ilmenite in Bushveld, unlike at some other VTM deposits (e.g. Rogaland, Norway: Duchesne, 1970; Emeishan, China: Tan et al., 2016). The mixed analyses show that V_2O_5 contents increase with increasing magnetite components from ∼ 1.19 wt % V_2O_5 at $X_{mt} = 0.27$ wt % to 2.4 wt % at $X_{mt} = 0.58$ (Fig. 7). Overall, cloth grains with lower-density ulvöspinel exsolution networks have higher V_2O_5 contents. Vanadium is therefore preferentially hosted in the magnetite component, but we believe that the compositional evolution we observe represents an evolution of the magma composition rather than a heterogeneous distribution of the ulvöspinel exsolution (Yuan et al., 2017) In any case, due to the pervasive cloth texture its degree of liberation is comparatively low. TiO_2 in magnetite increases with increasing mol fractions of ulvöspinel (X_{usp}), but, since the ulvöspinel lamellae are very thin, their liberation degree is low.

4 Ore processing

The microstructures of Ti- and V-containing minerals such as titanomagnetite, ilmenite, and vanadium bearing magnetite have a significant effect on the majority of the downstream ore processing (Guo et al., 2019; Wang et al., 2019). The most common structural properties include aspects such as mineralogical composition, grain size, intergrowths, microcracks, exsolutions, inclusions, oxidation states, and surface defects, as listed in a recent review considering the effects of ore textures (Månbro et al., 2025). Understanding these structures is essential for efficient downstream processing, and having control over them further increases chances for successful beneficiation. In different enrichment unit operations' optimized comminution does not only consume less energy but also enables efficient downstream processing. The success of gravity separation (e.g. sprials, shaking tables, or the Knelson concentrator) depends not only on grain size and shape and differences in density but also on the mineral association and liberation (Abaka-Wood et al., 2019). Thus, it can be generalized that well-liberated and intact grains behave optimally in gravity separation. Furthermore, structural differences in mineral grains define their magnetic properties (Zhitao and Kuangdi, 2022). As described above, the degree of oxidation is directly proportional to the degree of liberation for magnetite and ilmenite in the grains (Fig. 6). Consequently, these variations result in a distribution of varying magnetic susceptibility. Theoretically, proper characterization and control over different grain structures enable a higher separation efficiency in magnetic separation. The following sections highlight key processing aspects for the observed textures and provide a theoretical framework on their downstream processing.

4.1 Processing of sandwich and trellis textures

While the processing of the sandwich structure is partially more feasible compared to the cloth structure, it is still a challenging microstructure to process. The larger lamellas may be liberated through conventional grinding methods. However, new developments in ore processing are promising and could increase the degree of liberation. For example, use of high-pressure grinding mills (HPGR) (Guo et al., 2019) and microwave treatments (Wang et al., 2019) have been studied in an effort to break the ore structure along grain boundaries. According to Wang et al. (2019) the use of microwave treatment resulted in more cracks between grain boundaries, thus further enhancing grinding procedures and resulting in better liberation with coarser particle sizes. It is noteworthy that, in the processing of the sandwich and, especially, the trellis structures, the benefits of using HPGR or the microwave treatment will likely improve the efficiency of the downstream processing. While such novel methods improve liberation and can theoretically also expose the thin Ti lamellas in the sandwich structure, their efficient enriching relies heavily on their grain properties and the selected processing method, as discussed below.

Well-liberated larger ilmenite-containing grains from sandwich-textured magnetite can, theoretically, be separated through gravity separation. It can be assumed that the novel comminution methods mentioned above expose ilmenite surfaces, which also enables the use of froth flotation, especially for ilmenite. As a surface and adsorption-based separation technique, its performance depends heavily on proper liberation of valuable minerals (Bulatovic, 2007). In particular, the larger ilmenite inclusions can occupy most of the volume of a single 30–40 µm grain (depending on orientation). This, in turn, facilitates selective separation through flotation, while some gangue recovery is also to be expected depending on the actual grain size. However, another equally important aspect is the state of the surface minerals. For example, in the case of ilmenite flotation, the ratio between Fe^{2+} and Fe^{3+} determines the degree of interaction between the mineral surface and typical anionic collectors (such as sodium oleate) used in ilmenite flotation (Li et al., 2024). A further enhancement in the collector adsorption can be done by activating the ilmenite surfaces with sodium persulfate ($Na_2S_2O_8$), which reportedly prompts a conversion from Fe^{2+} into Fe^{3+} (Dai et al., 2025).

The trellis structure is expected to show the most promise in terms of enriching Ti and V in their own pre-concentrates. The larger grains can be exposed even through conventional comminution, while the novel methods further improve liberation and reduce energy consumption. When properly liberated, the larger ilmenite inclusions can be separated from the V-bearing magnetite through magnetic separation with relative ease compared to the more fine-grained structures. The ilmenite-rich non-magnetic fraction can be further enriched through froth flotation as the sizes of the ilmenite-bearing particles in the trellis structure are better suited for flotation (Wills and Finch, 2015).

4.2 Processing of cloth textures

As discussed above, the cloth structure contains thin needle-like exsolutions, which are notoriously difficult to liberate efficiently using conventional comminution techniques (Xu et al., 2017). With these methods, even a theoretical complete liberation of the cloth structure would result in overly fine particle sizes that are difficult or impossible to enrich – not to mention the immense energy demand of such operations (Baldassarre et al., 2020; Parapari, 2021). While some of the lamellas may be exposed when using HPGR or microwave treatment, a continuous cloth structure inhibits efficient separation in conventional enrichment unit operations. Structural changes occur in a sub-micrometre spacing, which results in a near-uniform structure throughout the cloth mineralization when considering processing methods such as gravity or magnetic separation. In addition, even with optimal reagents, flotation of the fine-grained ilmenite exsolutions is extremely difficult. In the typical size range where flotation is most effective (100–150 µm), the available surface area consisting of ilmenite is too small for the collectors to render the mineral surface sufficiently hydrophobic for them to attach to the bubbles in flotation. Conversely, if the particle size is very small (< 20 µm), gangue minerals can form slime coatings on top of the valuable minerals, effectively acting as depressants, while smaller particles also report to the concentrate more readily through the non-selective recovery of entrainment (Wills and Finch, 2015). Micro-flotation technologies of fine fractions could be a solution for a better recovery (Rulyov, 2016; Rulyov et al., 2020), but this still remains to be fully investigated.

4.3 Processing of a heterogeneous and complex ore

While Sect. 4.1 and 4.2 described the properties and typical processing behaviour of the distinct mineral structures present in the Bushveld Complex, in any realistic scenario it is impossible to segregate the processed ores based on their mineral structures to individual processing flow sheets. Accordingly, the efficient utilization and processing of this ore requires detailed planning throughout the beneficiation chain that simultaneously considers all structure types present in the complex. The resulting flow sheet should contain novel concepts, such as selective blasting and fragmentation combined with already existing technologies, like the HPGR, to maximize both the liberation and the energy efficiency of the comminution circuit. The subsequent downstream processing design should consider a series of varying unit operations, each designed for separate particle size ranges, from coarse to fine, with strategically positioned re-grinding stages, resulting in optimized energy consumption and separation efficiency.

5 Conclusions

This study demonstrates that magnetite–ilmenite microstructures in Bushveld VTM ores exert first-order control on both mineral chemistry and beneficiation performance. Oxidation-driven exsolution enriches vanadium in magnetite while partitioning titanium into ilmenite, creating strong intra-grain compositional gradients. Cloth textures, with their dense networks of ulvöspinel lamellae, limit effective liberation and reduce separation efficiency across magnetic, gravity, and flotation techniques. In contrast, sandwich and trellis textures present coarser, better-defined ilmenite lamellae that are more responsive to comminution and subsequent concentration. Nonetheless, trellis and sandwich textures remain challenging due to their pervasive, multidirectional intergrowths. However, using high-pressure grinding mills or microwave treatments will likely improve the efficiency of mineral liberation. These findings emphasize the need for detailed textural assessment prior to processing and support the development of texture-specific comminution and beneficiation strategies. Ultimately, the integration of microstructural and chemical insights offers a pathway towards improved recovery of V, Ti, and Fe from layered mafic intrusions.

Data availability. All of the underlying data of this study are available in the Supplement.

Supplement. The supplement related to this article is available online at https://doi.org/10.5194/ejm-38-545-2026-supplement.

Author contributions. ON and PM acquired funding. ON, PM, and TDvG conceptualized the paper. TDvG conducted the investigation, formal analyses, and data visualization. TDvG, TN, and ON wrote the initial paper, and PM, ON, TDvG and TN contributed to the review and editing.

Competing interests. The contact author has declared that none of the authors has any competing interests.

Disclaimer. Publisher's note: Copernicus Publications remains neutral with regard to jurisdictional claims made in the text, published maps, institutional affiliations, or any other geographical representation in this paper. The authors bear the ultimate responsibility for providing appropriate place names. Views expressed in the text are those of the authors and do not necessarily reflect the views of the publisher.

Acknowledgements. Bernard Charlier is thanked for the assistance during the field campaign. The authors thank Rucheng Wang for the editorial handling and Tan Wei and an anonymous reviewer for their insightful and constructive comments, which helped improve the paper.

Financial support. This research has been supported by the EU Horizon 2020 in the framework of the Horizon Europe AVANTIS project (grant no. 101137552).

Review statement. This paper was edited by Rucheng Wang and reviewed by Wei Tan and one anonymous referee.

References

Abaka-Wood, G. B., Quast, K., Zanin, M., Addai-Mensah, J., and Skinner, W.: A study of the feasibility of upgrading rare earth elements minerals from iron-oxide-silicate rich tailings using Knelson concentrator and Wilfley shaking table, Powder Technol., 344, 897–913, https://doi.org/10.1016/j.powtec.2018.12.005, 2019.

Andersen, D. J., Lindsley, D. H., and Davidson, P. M.: QUILF: A pascal program to assess equilibria among FeMgMnTi oxides, pyroxenes, olivine, and quartz, Comp. Geosci., 19, 1333–1350, https://doi.org/10.1016/0098-3004(93)90033-2, 1993.

Arguin, J. P., Pagé, P., Barnes, S. J., Girard, R., and Duran, C.: An integrated model for ilmenite, Al-spinel, and corundum exsolutions in titanomagnetite from oxide-rich layers of the Lac Doré complex (Québec, Canada), Minerals, 8, https://doi.org/10.3390/min8110476, 2018.

Baldassarre, G., Baietto, O., and Marini, P.: Comminution Effects on Mineral-Grade Distribution: The Case of an MVT Lead-Zinc Ore Deposit, Minerals, 10, https://doi.org/10.3390/min10100893, 2020.

Buddington, A. F. and Lindsley, D. H.: Iron-titanium oxide minerals and synthetic equivalents, J. Petrol., 5, 310–357, 1964.

Bulatovic, S. M.: Handbook of Flotation Reagents: Chemistry, Theory and Practice: Volume 1: Flotation of Sulfide Ores, Elsevier Science, Elsevier Science, https://doi.org/10.1016/B978-0-444-53029-5.X5009-6, 2007.

Carmichael, C. M.: The magnetic properties of ilmenite-haematite crystals, P. R. Soc. Lond. Ser. Math. Phys. Sci. Math. Phys. Sci., 263, 508–530, https://doi.org/10.1098/rspa.1961.0177, 1961.

Cawthorn, R.: The Bushveld Complex, South Africa, in: Layered Intrusions, edited by: Charlier, B., Namur, O., Latypov, R., and Tegner, C., Springer Geology, Springer, Dordrecht, https://doi.org/10.1007/978-94-017-9652-1_12, 2015.

Cawthorn, R. G. and Molyneux, T. G.: Vandafiferous magnetite deposits of the bushveld complex, in: Mineral Deposits of Southern Africa Vols I & II, edited by: Anhaeusser, C. R. and Maske, S., Geol. Soc. S. Afr., Johannesburg, 1251–1266, 1986.

Charlier, B., Namur, O., Duchesne, J.-C., Wiszniewska, J., Parecki, A., and vander Auwera, J.: Cumulate Origin and Polybaric Crystallization of Fe-Ti Oxide Ores in the Suwalki Anorthosite, Northeastern Poland, Econ. Geol., 104, 205–221, https://doi.org/10.2113/gsecongeo.104.2.205, 2009.

Charlier, B., Namur, O., Latypov, R., and Tegner, C.: Layered intrusions (1st edn.), Springer, https://doi.org/10.1007/978-94-017-9652-1, 2015a.

Charlier, B., Namur, O., Bolle, O., Latypov, R., and Duchesne, J. C.: Fe-Ti-V-P ore deposits associated with Proterozoic massif-type anorthosites and related rocks, Earth Sci. Rev., 141, 56–81, https://doi.org/10.1016/j.earscirev.2014.11.005, 2015b.

Dai, C., He, H., Chen, P., Yang, Y., Zhai, J., and Sun, W.: Surface modification of ilmenite with sodium persulfate and its effect on flotation performance, Appl. Surf. Sci., 680, 161354, https://doi.org/10.1016/j.apsusc.2024.161354, 2025.

Duchesne, J.-C.: Microtextures of Fe-Ti oxide minerals in the south-rogaland anorthositic complex (Norway), Ann. Soc. Belg., 93, 527–544, 1970.

Duchesne, J.-C.: Iron-Titanium Oxide Minerals in the Bjerkrem-Sogndal Massif, South-western Norway, J. Petrol., 13, 57–81, 1972.

Eales, H. V. and Cawthorn, R. G.: The Bushveld Complex. Layer, Intrusions, 15, 181–229, 1996.

Guo, X., Cui, S., Dai, S., Han, J., and Wang, C.: Investigation of microcrack formation in vanadium-titanium magnetite using different crushing processes, J. South. Afr. Insitute Min. Metall., 119, 811–816, 2019.

Haggerty, S. E.: Oxide textures – A mini-atlas, in: Reviews in Mineralogy, vol. 25: Oxide Minerals – Petrologic and Magnetic Significance, edited by: Lindsley, D. H., Mineralogical Society of America, Chantilly, 129–219, https://doi.org/10.1515/9781501508684-008, 1991.

Jarosewich, E.: Smithsonian Microbeam Standards, J. Res. Natl. Inst. Stand. Technol., 107, 681–685, http://www.nist.gov/jres (last access: 1 September 2025), 2002.

Kelley, K. D., Scott, C. T., Polyak, D. E., and Kimball, B. E.: Vanadium, in: Critical Mineral Resources of the United States—Economic and Environmental Geology and Prospects for Future Supply, edited by: Schultz, K. J., DeYoung, J. H., Seal II, R. R., and Bradley, D. C., Professional Paper 1802, US Geological Survey, Virginia, 797, https://doi.org/10.3133/pp1802U, 2017.

Latypov, R. M., Namur, O., Bai, Y., Barnes, S. J., Chistyakova, S. Y., Holness, M. B., Iacono-Marziano, G., Kruger, W. A. J., O'Driscoll, B., Smith, W. D., Virtanen, V. J., Wang, C. Y., Xing, C. M., and Charlier, B.: Layered intrusions: Fundamentals, novel observations and concepts, and controversial issues, Earth Sci. Rev., 249. https://doi.org/10.1016/j.earscirev.2023.104653, 2024.

Li, J., He, H., Shao, Y., Liu, C., Li, R., Chen, H., and Meng, X.: Efficient Flotation Separation of Ilmenite and Olivine in a Weak Alkaline Pulp Using a Ternary Combination Collector Centered around Al3+, Molecules, 29, https://doi.org/10.3390/molecules29184379, 2024.

Lindsley, D. H.: Experimental studies of oxide minerals, in: Oxide Minerals, Reviews in Mineralogy and Geochemistry, edited by: Lindsley, D. H., 69–106, Walter de Gruyter. https://doi.org/10.1515/9781501508684-006, 1991.

Månbro, C., Parian, M., and Rosenkranz, J.: Exploring the role of ore texture in comminution and approaches to identify and promote non-random breakage, Miner. Eng., 230, 109405, https://doi.org/10.1016/j.mineng.2025.109405, 2025.

Mathison, C. I. and Ahmat, A. L.: The Windimurra Complex, Western Australia, Layer, Intrusions, 15, 485–510, 1996.

Molyneux, T. G.: A Geological investigation of the Bushveld complex in Sekhukhuneland and part of the steelport valley, Trans. Geol. Soc. South Afr., 77, 329–338, 1974.

Mücke, A.: Magnetite, ilmenite and ulvite in rocks and ore deposits: petrography, microprobe analyses and genetic implications, Mineral. Petrol., 77, 215–234, https://doi.org/10.1007/s00710-002-0216-1, 2003.

Namur, O. and Charlier, B.: Efficiency of compaction and compositional convection during mafic crystal mush solidification: the Sept Iles layered intrusion, Canada, Contrib. Mineral. Petrol., 163, 1049–1068, 2012.

Namur, O. and Humphreys, M. C. S.: Trace Element Constraints on the Differentiation and Crystal Mush Solidification in the Skaergaard Intrusion, Greenland, J. Petrol., 59, 387–418, https://doi.org/10.1093/petrology/egy032, 2018.

Namur, O., Charlier, B., Toplis, M. J., Higgins, M. D., Liégeois, J. P., and vander Auwera, J.: Crystallization sequence and magma chamber processes in the ferrobasaltic Sept Iles layered intrusion, Canada, J. Petrol., 51, 1203–1236, https://doi.org/10.1093/petrology/egq016, 2010.

Namur, O., Abily, B., Boudreau, A. E., Blanchette, F., Bush, J. W. M., Ceuleneer, G., Charlier, B., Donaldson, C. H., Duchesne, J.-C., Higgins, M. D., Morata, D., Nielsen, T. F. D., O'Driscoll, B., Pang, K. N., Peacock, T., Spandler, C. J., Toramaru, A., and Veksler, I. V.: Igneous layering in basaltic magma chambers, in: Layered Intrusions, edited by: Charlier, B., Namur, O., Latypov, R., and Tegner, C., Springer Geology, Dordrecht, 75–152, https://doi.org/10.1007/978-94-017-9652-1, 2015.

Parapari, P. S.: Efficient mineral liberation – Multidimensional investigation of mechanical stress and ore texture, Ph.D. Dissertation, Luleå University of Technology, 2021.

Price, G. D.: Exsolution microstructures in titanomagnetites and their magnetic significance, Phys. Earth Planet. Inter., 23, 2–12, https://doi.org/10.1016/0031-9201(80)90078-3, 1980.

Ramdohr, P.: Ulvöspinel and its significance in titaniferous iron ores, Econ. Geol., 48, 677–688, 1953.

Reynolds, I. M.: The Nature and Origin of Titaniferous Magnetite-Rich Layers in the Upper Zone of the Bushveld Complex: A Review and Synthesis, Econ. Geol., 80, 1089–1108, https://doi.org/10.2113/gsecongeo.80.4.1089, 1985.

Rulyov, N. N.: Combined microflotation of fine minerals: theory and experiment, Miner. Process. Extr. Metall., 125, 81–85, https://doi.org/10.1080/03719553.2016.1156303, 2016.

Rulyov, N. N., Filippov, L. O., and Kravchenko, O. V.: Combined microflotation of glass beads, Colloids Surf. Physicochem. Eng. Asp., 598, 124810, https://doi.org/10.1016/j.colsurfa.2020.124810, 2020.

Scoon, R. N. and Mitchell, A. A.: The upper zone of the bushveld complex at roossenekal, south africa: Geochemical stratigraphyand evidence of multiple episodes of magma replenishment, South Afr. J. Geol., 115, 515–534, https://doi.org/10.2113/gssajg.115.4.515, 2012.

Shepherd, K., Namur, O., Toplis, M. J., Devidal, J. L., and Charlier, B.: Trace element partitioning between clinopyroxene, magnetite, ilmenite and ferrobasaltic to dacitic magmas: an experimental study on the role of oxygen fugacity and melt composition, Contrib. Mineral. Petrol., 177, 1–21, https://doi.org/10.1007/s00410-022-01957-y, 2022.

Spencer, K. J. and Lindsley, D. H.: A solution model for coexisting iron-titanium oxides, Am. Mineral., 66, 1189–1201, 1981.

Tan, W., Liu, P., He, H., Wang, C. Y., and Liang, X.: Mineralogy and origin of exsolution in Ti-rich magnetite from different magmatic Fe-Ti oxide-bearing intrusions, Can. Mineral., 54, 539–553, https://doi.org/10.3749/canmin.1400069, 2016.

Taner, M. F., Ercit, T. S., and Gault, R. A.: Vanadium-bearing Magnetite from the Matagami and Chibougamau Mining Districts, Abitibi, Quebec, Canada, Explor. Min. Geol., 7, 299–311, 1998.

Taylor, C. D., Schulz, K. J., Doebrich, J. L., Orris, G. J., Denning, P. D., Kirschbaum, M. J., and Myers, M. D.: Geology and Nonfuel Mineral Deposits of Africa and the Middle East, U. S. Geological Survey Open-File Report 2005–1294-E, 2009.

Taylor, P. R., Shuey, S. A., Vidal, E. E., and Gomez, J. C.: Extractive metallurgy of vanadium-containing titaniferous magnetite ores: A review, Miner. Metall. Process., 23, 80–86, https://doi.org/10.1007/bf03403340, 2006.

Turnock, A. and Eugster, H. P.: Fe-Al Oxides : Phase Relationships below 1000C, J. Petrol., 3, 533–564, 1962.

Von Gruenewaldt, G., Klemm, D. D., Henckel, J., and Dehm, R. M.: Exsolution features in titanomagnetites from massive magnetite layers and their host rocks of the upper zone, eastern Bushveld complex, Econ. Geol., 80, 1049–1061, https://doi.org/10.2113/gsecongeo.80.4.1049, 1985.

Wang, J., Jiang, T., Liu, Y., and Xue, X.: Influence of microwave treatment on grinding and dissociation characteristics of vanadium titano-magnetite, Int. J. Miner. Metall. Mater., 26, 160–167, https://doi.org/10.1007/s12613-019-1720-1, 2019.

Wills, B. A. and Finch, J. A.: Chapter 12 – Froth Flotation, in: Wills' Mineral Processing Technology, 8th edn., edited by: Wills, B. A. and Finch, J. A., Butterworth-Heinemann, Boston, 265–380, https://doi.org/10.1016/B978-0-08-097053-0.00012-1, 2015.

Xu, C., Zhang, Y., Liu, T., and Huang, J.: Characterization and Pre-Concentration of Low-Grade Vanadium-Titanium Magnetite Ore, Minerals, 7, https://doi.org/10.3390/min7080137, 2017.

Yuan, Q., Namur, O., Fischer, L. A., Roberts, R. J., Lü, X., and Charlier, B.: Pulses of plagioclase-laden magmas and stratigraphic evolution in the Upper Zone of the Bushveld Complex, South Africa, J. Petrol., 58, 1619–1644, https://doi.org/10.1093/petrology/egx067, 2017.

Zeh, A., Ovtcharova, M., Wilson, A. H., and Schaltegger, U.: The Bushveld Complex was emplaced and cooled in less than one million years – results of zirconology, and geotectonic implications, Earth Planet. Sc. Lett., 418, 103–114, https://doi.org/10.1016/j.epsl.2015.02.035, 2015.

Zhitao, Y. and Kuangdi, X.: Mineral Magnetism, in: Xu, K. (Ed.), The ECPH Encyclopedia of Mining and Metallurgy, Springer Nature Singapore, Singapore, 1–2, https://doi.org/10.1007/978-981-19-0740-1_475-1, 2022.

Zhou, M. F., Robinson, P. T., Lesher, C. M., Keays, R. R., Zhang, C. J., and Malpas, J.: Geochemistry, petrogenesis and metallogenesis of the panzhihua gabbroic layered intrusion and associated Fe-Ti-V Oxide deposits, sichuan province, SW China, J. Petrol., 46, 2253–2280, https://doi.org/10.1093/petrology/egi054, 2005.